Exciton binding energy and subband structures of GaAs/$Al_xGa_{1-x}As$ superlattices

D. S. Chuu and Ying-Chih Lou
Department of Electrophysics, National Chiao Tung University, Hsinchu, Taiwan, Republic of China
(Received 18 September 1990; revised manuscript received 17 December 1990)

The subband structure and the binding energy of an exciton in the GaAs/$Al_xGa_{1-x}As$ superlattice are studied by a simple approximation method. Both the exciton binding energy and the subband energy are expressed as a function of well width, barrier width, and Al composition. The influence of the effective-mass mismatch is taken into account. The energy spacings between interband or intersubband transitions are calculated and compared with the observed data. Good agreement is obtained.

I. INTRODUCTION

In recent years, the techniques of molecular-beam epitaxy (MBE) and metal-organic chemical-vapor deposition (MOCVD) have been used to grow high-quality heterojunctions; thus the growth of the systems consisting of alternate layers of two different semiconductors with controllable thicknesses has become possible. These heterostructures have stimulated new works in semiconductor physics over the past ten years. For example, we are now able to control layers so thin that some quantum-confinement effects of electrons and holes can readily be seen. For example, in bulk GaAs, the exciton resonances are very weak and thus can be observed only at very low temperatures. However, in the superlattices, the exciton resonances become considerably sharp due to the quantum-confinement effect and thus can be observed easily at room temperature. In recent years, the exciton problems in semiconductor quantum wells and superlattice structures have been studied extensively.[1–22] This is because a knowledge of the exciton binding energy is crucial to the interpretation of the photoluminescence spectra and photoluminescence excitation spectra, which are used to determine the excitonic properties of the heterostructures.[1] Most of the recent works are concerned with the excitonic binding energies[2–4] in double quantum wells or superlattices and the optical properties and spectroscopy[5–9] in superlattices. Moore *et al.*[4] recently presented a direct measurement of the heavy-hole exciton binding energy in a III-V compound quantum-well system, where the well widths are 25 Å or smaller. Recently, Mo and Sung[10] reported extensive calculations on several variants of the single-subband model. Dignam and Sipe[11] proposed an approach to variationally calculate the binding energy for both types-I and -II superlattices. In theoretical calculations of the exciton binding energies, it is customary to employ the infinite-barrier model and the effective-mass approximation. It is known that the heterojunction formed between two dissimilar semiconductors may cause a position-dependent effective mass.[23–28] Therefore, the influence of the effective-mass mismatch should be properly taken into account if the effective-mass approximation is used in the calculation. Recently, the proper form of the kinetic-energy operator and the boundary conditions for the effective-mass theory[23–28] have been established.

In this work, we will employ a simple approximation method which in some cases combines the spirit of the perturbative- and variational-principle approaches to study the subband structures and the exciton binding energies of a superlattice system. The dependence of the subband energies on the well width, barrier width, Al composition, and temperature will be studied. The influence of the effective-mass mismatch will be considered. In this work, the GaAs/$Al_xGa_{1-x}As$ superlattice is chosen for illustration. This is because the observed data for GaAs/$Al_xGa_{1-x}As$ superlattice are more abundant.[1,5–8,15]

II. THEORY

The Hamiltonian for an exciton in the GaAs/$Al_xGa_{1-x}As$ superlattice system in the effective-mass approximation can be expressed as follows:

$$\mathcal{H}=-\frac{\partial}{\partial x_e}\frac{\hbar^2}{2m_{e\rho}(z_e)}\frac{\partial}{\partial x_e}-\frac{\partial}{\partial y_e}\frac{\hbar^2}{2m_{e\rho}(z_e)}\frac{\partial}{\partial y_e}-\frac{\partial}{\partial z_e}\frac{\hbar^2}{2m_{eZ}(z_e)}\frac{\partial}{\partial z_e}+V_e(z_e)-\frac{\partial}{\partial x_h}\frac{\hbar^2}{2m_{m\rho}(z_h)}\frac{\partial}{\partial x_h}$$
$$-\frac{\partial}{\partial y_h}\frac{\hbar^2}{2m_{h\rho}(z_h)}\frac{\partial}{\partial y_h}-\frac{\partial}{\partial z_h}\frac{\hbar^2}{2m_{hZ}(z_h)}\frac{\partial}{\partial z_h}+V_h(z_h)+V_{e\text{-}h}\ , \tag{1}$$

where the kinetic-energy operator is suggested by Von Roos,[26] and

$$V_{e\text{-}h}=-\frac{e^2}{\epsilon[(x_e-x_h)^2+(y_e-y_h)^2+(z_e-z_h)^2]^{1/2}}$$

is the Coulomb interaction between the electron and hole, $m_{e\rho}$ ($m_{h\rho}$) is the electron (hole) effective mass along the x or y direction, and m_{eZ} (m_{hZ}) is the electron (hole) effective mass along the z direction (the z direction is defined as the direction perpendicular to the heterojunctions). These masses will, in general, depend on z. V_e (V_h) is the electron (hole) confining potential set up by the heterojunctions. Equation (1) cannot be solved exactly. Let us first set

$$x=x_e-x_h,\quad y=y_e-y_h,\quad z=z_e-z_h\ ,$$
$$\rho^2=x^2+y^2,\quad r^2=x^2+y^2+z^2\ ,$$
$$1/\mu=1/m_{h\rho}(z_h)+1/m_{e\rho}(z_e)\ .$$

Then the Hamiltonian can be rewritten as

$$\begin{aligned}\mathcal{H}=&-\frac{\partial}{\partial z_e}\frac{\hbar^2}{2m_{eZ}(z_e)}\frac{\partial}{\partial z_e}+V_e(z_e)\\&-\frac{\partial}{\partial z_h}\frac{\hbar^2}{2m_{hZ}(z_h)}\frac{\partial}{\partial z_h}+V_h(z_h)\\&-\frac{\hbar^2}{2\mu}\left[\frac{\partial^2}{\partial x^2}+\frac{\partial^2}{\partial y^2}\right]-\frac{e^2}{\epsilon r}\ .\end{aligned}\tag{2}$$

In the above equation the center-of-mass motion in the x-y plane, whose free motion can be decoupled from the other, has been omitted. The exact eigenfunctions of $\mathcal{H}$ are still difficult to obtain. We now introduce a parameter λ into Eq. (2) by adding and subtracting a term $\lambda e^2/\epsilon\rho$ from $\mathcal{H}$ and rearrange $\mathcal{H}$ as

$$\mathcal{H}=\mathcal{H}_{z_e}+\mathcal{H}_{z_h}+\mathcal{H}_{xy}(\lambda)+\mathcal{H}'(\lambda)=\mathcal{H}_0(\lambda)+\mathcal{H}'(\lambda)\ ,\tag{3}$$

where

$$\mathcal{H}_{z_e}=-\frac{\partial}{\partial z_e}\frac{\hbar^2}{2m_{eZ}(z_e)}\frac{\partial}{\partial z_e}+V_e(z_e)\ ,\tag{4a}$$

$$\mathcal{H}_{z_h}=-\frac{\partial}{\partial z_h}\frac{\hbar^2}{2m_{hZ}(z_h)}\frac{\partial}{\partial z_h}+V_h(z_h)\ ,\tag{4b}$$

$$\mathcal{H}_{xy}(\lambda)=-\frac{\hbar^2}{2\mu}\left[\frac{\partial^2}{\partial x^2}+\frac{\partial^2}{\partial y^2}\right]-\frac{\lambda e^2}{\epsilon\rho}\ ,\tag{4c}$$

$$\mathcal{H}'(\lambda)=\frac{\lambda e^2}{\epsilon\rho}-\frac{e^2}{\epsilon r}\ .\tag{4d}$$

The first three parts of $\mathcal{H}(\lambda)$, i.e., $\mathcal{H}_0(\lambda)$, $\mathcal{H}_{z_e}$, H_{z_h}, and $\mathcal{H}_{xy}$, are functions of z_e, z_h, and ρ, respectively, and thus can be solved separately. Both $\mathcal{H}_{z_e}$ and $\mathcal{H}_{z_h}$ in Eq. (3) are the Hamiltonian for one-dimensional (1D) periodic square-well-potential system (Kronig-Penny model) with position-dependent effective mass and can be solved exactly. The Hamiltonian $\mathcal{H}_{xy}(\lambda)$ in Eq. (3) is equivalent to that of a two-dimensional (2D) hydrogenic system[29] and can be solved exactly too. After solving the Schrödinger equation for $\mathcal{H}_0(\lambda)$, the total eigensolutions for $\mathcal{H}(\lambda)$ can be obtained by the perturbation method. The parameter λ contained in $\mathcal{H}(\lambda)$ can be determined by requiring the minimum variation of the total eigen energy with λ [i.e., $\partial E(\lambda)/\partial\lambda=0$]. We will solve for $\mathcal{H}_0(\lambda)$ first as follows.

A. The solution for the 1D periodic square-well-potential system

The Schrödinger equation for $\mathcal{H}_{z_e}$ and $\mathcal{H}_{z_h}$ can be written as follows:

$$-\frac{\partial}{\partial z}\frac{\hbar^2}{2m_z(z)}\frac{\partial f}{\partial z}+V(z)f=\mathcal{E}f\ ,$$

where

$$V(z)=\begin{cases}V_0 & \text{for } z \text{ inside the barrier,}\\ 0 & \text{for } z \text{ inside the well.}\end{cases}$$

(i) The eigenfunction in the region $-a/2<z<a/2$ (inside the well) can be expressed as

$$f_a=A\cos(kz)+B\sin(kz)\tag{5}$$

with $\mathcal{E}=\hbar^2k^2/2m_{\alpha z}$, where $m_{\alpha z}$ is the effective mass for the electron (or hole) inside the well.

(ii) The solution in the region $-a/2-b<z<-a/2$ (inside the barrier) can be expressed as

$$f_\beta=Ce^{Q[z+(a+b)/2]}+De^{-Q[z+(a+b)/2]}\ ,\tag{6a}$$

with $V_0-\mathcal{E}=\hbar^2Q^2/2m_{\beta z}$, where $m_{\beta z}$ is the effective mass for the electron (or hole) inside the barrier. In the region $-a/2<z<a/2+b$, the solution is related to Eq. (6a) by the Bloch theorem

$$\begin{aligned}&f_\beta(-a/2<z<a/2+b)\\&\quad=f_\beta(-a/2-b<z<-a/2)e^{ik(a+b)}\ .\end{aligned}\tag{6b}$$

The boundary conditions require f_α and f_β continue at $z=a/2$ and $z=-a/2$; and $(1/m_{\alpha z})\partial f_\alpha/\partial z$ and $(1/m_{\beta z})\partial f_\beta/\partial z$ continue at $z=a/2$ and $-a/2$, respectively. These boundary conditions yield two sets of equations that can be used to obtain the eigenenergies of the 1D periodic square-well-potential system as usual treatment.

B. The solution for the 2D hydrogenic system

The Schrödinger equation for $\mathcal{H}_{xy}(\lambda)$ can be expressed as

$$-\frac{\hbar^2}{2\mu}\left[\frac{\partial^2}{\partial x^2}+\frac{\partial^2}{\partial y^2}\right]\phi-\frac{\lambda e^2}{\epsilon\rho}\phi=\mathcal{E}\phi\ ;$$

the solution can be expressed as

$$\phi_{j,|l|}(\rho,\theta;\lambda)=\frac{1}{\sqrt{2\pi}}\exp(i|l|\theta)\times\left[\frac{(j+|l|)!}{[(j+|l|)!]^3(2j+1)}\times\left[\frac{2}{(j+\frac{1}{2})\alpha_0}\right]^2\right]^{1/2}\times\rho^{|l|}\exp(-\rho/2)L^{2|l|}_{j+|l|}(\rho) \quad (7)$$

and

$$\mathcal{E}_j=-\frac{\lambda^2 R}{(j+\frac{1}{2})^2} \quad (8)$$

with $j=0,1,2,\ldots,$ and $l=0,\pm1,\pm2,\ldots,\pm j$. $L^{2|l|}_{j+|l|}(\rho)$ is the associated Laguerre polynomial, where $\rho=2\lambda r/[(j+1/2)\alpha_0]$ and $\alpha_0=\epsilon\hbar^2/(\mu e^2)$ is the transverse effective Bohr radius, and $R=\mu e^4/(2\hbar^2\epsilon^2)$ is the three-dimensional effective Rydberg calculated with transverse reduced mass μ. It is known that the transverse effective masses in heterostructures are different in barrier layers and in well layers. To take into account this effective-mass mismatch, μ can be replaced by the equivalent transverse effective mass μ^*. We commonly use the average value of the transverse effective mass in the barrier and the well with the weight factors being the probabilities of finding the particle inside and outside the well as the equivalent transverse effective mass. The expression of μ^* can be obtained as follows.

Consider an electron in a conduction band or a hole in a valence band of a superlattice system. The Hamiltonian inside and outside the quantum well can be approximated by

$$\mathcal{H}_\alpha=\frac{\mathcal{P}_x^2+\mathcal{P}_y^2}{2m_{\alpha\rho}}+\frac{\mathcal{P}_z^2}{2m_{\alpha z}} \quad (9a)$$

and

$$\mathcal{H}_\beta=\frac{\mathcal{P}_x^2+\mathcal{P}_y^2}{2m_{\beta\rho}}+\frac{\mathcal{P}_z^2}{2m_{\beta z}}+V\ , \quad (9b)$$

respectively, where $m_{\alpha\rho}$ ($m_{\alpha z}$) and $m_{\beta\rho}$ ($m_{\beta z}$) are the bulk transverse (longitudinal) effective masses of semiconductors α and β. The wave function of the system can still be factorized as $\psi(r)=f(z)\exp(i\mathbf{k}_\rho\cdot\rho)$, where ρ is the position vector in the x-y plane. The problem then reduces to a Schrödinger equation for $f(z)$, and this equation is the same as we solved above. Its ground-state wave function is of the form

$$f(z)=A\cos(kz)\ ,$$

for

$$-a/2\pm n(a+b)<z<a/2\pm n(a+b)\ ,$$

with $\mathcal{E}_z=\hbar^2k^2/(2m_{\alpha z})$, and

$$f(z)=C(e^{Q[z+(a+b)/2]}+e^{-Q[z+(a+b)/2]})\ ,$$

for

$$(-a/2-b)\pm n(a+b)<z<-a/2\pm n(a+b)\ ,$$

with

$$V-\mathcal{E}_z=\frac{\hbar^2Q^2}{2m_{\beta z}}\ ,$$

and

$$(k/m_{\alpha z})\tan(ka/2)=(Q/m_{\beta z})\tanh(Qb/2),$$

a (b) is the width of well (barrier). Using the continuity conditions (ψ and $\partial\psi/\partial x$ continue) in the interface between α and β, it is easy to obtain $k_{\alpha\beta}=k_{\beta\rho}\equiv k_\rho$. Thus the eigenenergy of our system can be expressed as

$$\mathcal{E}=\hbar^2k_\rho^2/2m_{\alpha\rho}+\hbar^2k^2/2m_{\alpha z}\ .$$

Using above equations and the definition of transverse effective mass at $k_\rho=0$

$$\frac{1}{m_\rho^*}=\frac{1}{\hbar^2}\frac{\partial^2\mathcal{E}}{\partial k_\rho^2}\bigg|_{k_\rho=0}\ , \quad (10)$$

the equivalent transverse effective mass m_ρ^* for the even and odd solutions can be obtained as

$$\frac{1}{m_\rho^*}=\frac{1}{m_{\alpha\rho}}\pm\frac{k(m_{\alpha\rho}-m_{\beta\rho})}{m_{\alpha\rho}m_{\beta\rho}}\left[\frac{(1/w)\tanh(bw/2)+(b/2)\operatorname{sech}^2(bw/2)}{\tan(ka/2)\pm(ka/2)\sec^2(ka/2)\pm(k/w)\tanh(bw/2)\pm(bk/2)\operatorname{sech}^2(bw/2)}\right]\ , \quad (11)$$

where

$$w=\left[\frac{2m_{\beta z}}{\hbar^2}\left[V-\frac{\hbar^2k^2}{2m_{\alpha z}}\right]\right]^{1/2}\ ,$$

and $\mu^*=m_{e\rho}^*m_{h\rho}^*/(m_{e\rho}^*+m_{h\rho}^*)$.

C. The solution of total Hamiltonian H

From the above discussions, the eigensolutions of the unperturbed part $\mathcal{H}_0(\lambda)$ can be expressed as

$$\psi_n^{(0)}(r;\lambda)=f_e(z_e)f_h(z_h)\phi_{j,|l|}(\rho,\theta;\lambda)\ , \quad (12)$$

and

$$\mathcal{E}_n^{(0)}(\lambda)=\frac{\hbar^2 k_e^2}{2m_{eZ}}+\frac{\hbar^2 k_h^2}{2m_{hz}}-\frac{\lambda^2}{(j+\frac{1}{2})^2}\frac{\mu^* e^4}{2\epsilon^2\hbar^2}\ , \tag{13}$$

where f_e, f_h, $\phi_{j,|l|}$ are solutions of $\mathcal{H}_{z_e}$, $\mathcal{H}_{z_h}$ and $\mathcal{H}_{xy}$; μ^* is the equivalent transverse reduced mass, and k_e and k_h can be obtained from the boundary conditions mentioned in the Sec. II A. The solutions for the total Hamiltonian $\mathcal{H}$ can then be obtained by the formula of the conventional perturbation method:

$$\mathcal{E}_n=\mathcal{E}_n^{(0)}(\lambda)+\Delta\mathcal{E}_n(\lambda)\ , \tag{14a}$$

where

$$\Delta\mathcal{E}_n(\lambda)=\langle\psi_n^{(0)}(\lambda)|\mathcal{H}'(\lambda)|\psi_n\rangle \tag{14b}$$

with the normalization condition

$$\langle\psi_n^{(0)}(\lambda)|\psi_n\rangle=1 \tag{14c}$$

and ψ_n is the exact solution of $\mathcal{H}$ which can be expressed as

$$\psi_n=\psi_n^{(0)}(\lambda)+\Delta\psi_n(\lambda) \tag{14d}$$

and

$$|\Delta\psi_n(\lambda)\rangle=\sum_{m\neq n}{}'\frac{|\psi_m^{(0)}(\lambda)\rangle\langle\psi_m^{(0)}(\lambda)|\mathcal{H}'(\lambda)|\psi_n\rangle}{\mathcal{E}_n-\mathcal{E}_m^{(0)}(\lambda)}\ . \tag{14e}$$

In a practical calculation, we use $\psi_n^{(0)}(\lambda)$ in Eq. (12) to approximate the exact solution ψ_n in Eq. (14b). Then the parameter λ is determined by requiring minimal sensitivity[30] of $E_n(\lambda)$ with respect to λ [i.e., set $\partial\mathcal{E}_n(\lambda)/\partial\lambda=0$]. After λ is determined, $\Delta\psi_n(\lambda)$ in Eq. (14e) and $\Delta\mathcal{E}_n(\lambda)$ in Eq. (14b) can thus be obtained. Therefore, a more exact $\mathcal{E}_n(\lambda)$ can be finally calculated from Eq. (14a). The exciton binding energy $\mathcal{E}_{ex}$ can be obtained as follows:

$$\mathcal{E}_{ex}=\mathcal{E}_n-\frac{\hbar^2 k_e^2}{2m_{eZ}}+\frac{\hbar^2 k_h^2}{2m_{hz}}\ . \tag{15a}$$

The energy of a photon emitted in the recombination of an exciton can be defined as

$$\mathcal{E}_q=\mathcal{E}_n+\mathcal{E}_{gap}\ , \tag{15b}$$

where $\mathcal{E}_{gap}$ is the bulk energy gap of semiconductor in GaAs layers. $\mathcal{E}_q$ can be measured by the linear optical spectroscopic techniques, such as absorption, luminescence, and modulation spectroscopy.

III. RESULTS AND DISCUSSIONS

Consider the z axis of the GaAs/$Al_xGa_{1-x}As$ superlattices along the [100] direction. Thus, for $x<0.45$, $Al_xGa_{1-x}As$ has a direct band gap $\mathcal{E}_g(x)$ at the Γ point.[31] The bulk material parameters of $Al_xGa_{1-x}As$ and GaAs are available experimentally[31] for some x, and the entire range of x can be obtained by the interpolation. It was found that the band gap varies with both the composition x and the temperature.[12] At room temperature ($T=300$ K) and for $x<0.45$, the band gap has been determined[31] as $\mathcal{E}_g(x)=1.424+1.247x$ eV, and its temperature coefficient follows $\partial\mathcal{E}_g(x)/\partial T=-0.395-0.115x$ meV/K. The static dielectric constant is $\epsilon/\epsilon_0=13.18-3.12x$, and the effective mass of an electron in the conduction band is generally accepted[31] as $m_e/m_0=0.0665+0.0835x$ (m_0 is the free electron rest mass). However, the effective masses of both heavy and light holes in the valence band have different measured values in the [100] and [111] directions. Thus, the effective mass of holes is anisotropic in bulk $Al_xGa_{1-x}As$ and has been determined[32–34] as follows: heavy-hole effective mass perpendicular to the junction, $m_{hz}/m_0=0.45+0.31x$; light-hole effective mass perpendicular to the junction, $m_{lz}/m_0=0.088+0.049x$; heavy-hole effective mass parallel to the junction, $m_{h\rho}/m_0=(1/4m_{hz}+3/4m_{lz})^{-1}$; light-hole effective mass parallel to the junction, $m_{l\rho}/m_0=(1/4m_{lz}+3/4m_{hz})^{-1}$.

TABLE I. $C1$-$H1$ and $C1$-$L1$ interband transitions for different GaAs/$Al_xGa_{1-x}As$ superlattice systems. The notation Cm-$H(L)n$ denotes transitions from mth conduction subband to nth valence subband of heavy- (H) or light- (L) hole character.

				$C1$-$H1$ (meV)		$C1$-$L1$ (meV)	
L_w/L_b (Å)	Temp. (K)	χ	E_g (meV)	Expt.	Calc.	Expt.	Calc.
90/100	3	0.25	1519	1552	1555	1566	1569
116/100	3	0.25	1519	1540	1542	1551	1557
150/100	3	0.25	1519	1530	1533	1538	1542
210/100	3	0.25	1519	1522	1525	1527	1530
315/100	3	0.25	1519	1516	1520	1520	1524
90/25	3	0.25	1519	1545	1547	1556	1561
150/25	3	0.25	1519	1530	1532	1538	1542
71/71	300	0.18	1424	1467	1468	1479	1480
71/99	300	0.18	1424	1469	1470	1479	1480
71/150	300	0.18	1424	1469	1470	1480	1480
71/210	300	0.18	1424	1469	1471	1479	1481
100/150	300	0.3	1424	1453	1455	1465	1469

TABLE II. Interband transitions Cn-$H(L)n$, $n=1,2,3,4$, between higher-order subbands for GaAs/$Al_{0.24}Ga_{0.76}$As superlattices with L_w (well width)=220 Å, L_b (barrier width)=150 Å, and $T=300$ K, where Cm-$H(L)$ denotes transitions from mth conduction subband to nth valence subband of heavy- (H) or light- (L) hole character.

Transition	Expt. (meV)	Calc. (meV)
$C1$-$H1$	1426±1	1429
$C1$-$L1$	1430±5	1438
$C2$-$H2$	1456±2	1458
$C2$-$H2$	1474±5	1480
$C3$-$H3$	1510±3	1508
$C3$-$H3$	1541±5	1550
$C4$-$H4$	1576±3	1576
$C4$-$H4$	1626±5	1639

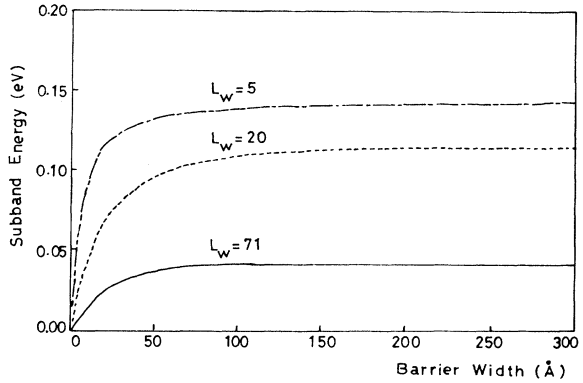

FIG. 1. Variation of the energy difference (in eV) between the first conduction subband and the conduction-band edge with barrier width L_b (in Å) for three well widths: $L_w=5$, 20, 71 Å.

There is a parameter, the conduction-band offset coefficient Q, which cannot be measured from experiment. Fu and Chao[34] have solved the one-dimensional multiple quantum wells of the GaAs/Al_xGa_{1-x}As system and fit their calculated results to optical data by adjusting Q. They obtain good fits when $Q=0.65$ is used. Pollak and Shen[5] also find that the best agreement between the observed and theoretical data was achieved for $Q=0.65$. In this work the conduction-band offset coefficient $Q=0.65$ is chosen.

It is known that knowledge of the interband and intersubband transitions of superlattices is very important in the electro-optic applications. These transitions will be influenced notably by the exciton binding energy because of quantum confinement. There are several experiments[1,5–8,15] that use the linear optical spectroscopic techniques to measure the interband and intersubband transitions of GaAs/Al_xGa_{1-x}As superlattices and find that the transitions depend not only on the widths of the well and barrier but also depend on the temperature and the Al composition x. Tables I–III list our calculated results by Eq. (15) under the same conditions as those of experimental observations. The notation Cm-$H(L)n$ shown in the tables denotes transitions from mth conduction subband to nth valence subband of heavy- (H) or light- (L) hole character. Table I lists our calculated results for $C1$-$H1$ and $C1$-$L1$, and some available experimental data[23,26] are also listed for comparison. One can see that good agreement can be obtained for different well width

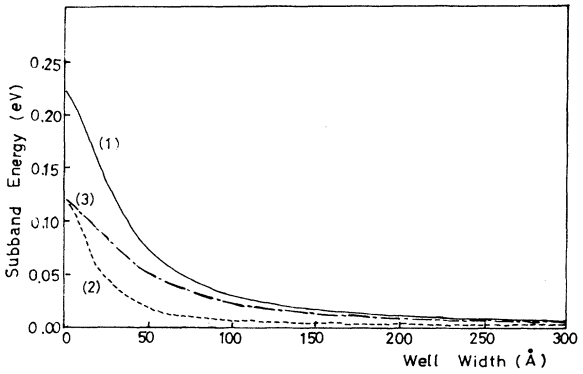

FIG. 2. Variation of the first subband energy (in eV) of the electron [curve (1)]; the energy difference (in eV) between the valence-band edge and the heavy-hole [curve (2)] and light-hole subbands [curve (3)] with well width (in Å).

TABLE III. Intersubband transitions $C1$-$C2$ and $C1$-$C3$ for GaAs/Al_xGa_{1-x}As superlattices with $x=0.3$, the well width $L_w=191$ Å, barrier width $L_b=199$ Å, and $T=3$ K. Cm-$H(L)n$ denotes transitions from mth conduction subband to nth valence subband of heavy- (H) or light- (L) hole character.

Transition	Expt. (meV)	Calc. (meV)
$C1$-$C2$	31.6±1.5	33.2
$C1$-$C3$	91.7±1.0	88.1

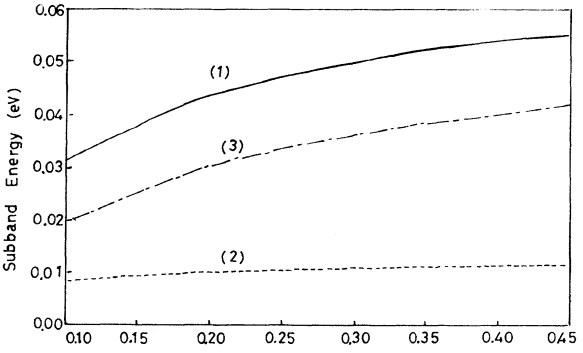

FIG. 3. Variation of the first subband energy (in eV) of the electron [curve (1)]; the energy difference (in eV) between the valence-band edge and the heavy-hole subband [curve (2)] and light-hole subbands [curve (3)] with Al composition x.

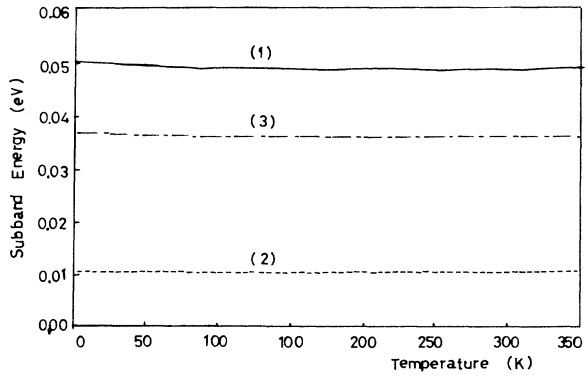

FIG. 4. Variation of the first subband energy (in eV) of the electron [curve (1)]; the energy difference (in eV) between the valence-band edge and the heavy-hole [curve (2)] and light-hole subbands [curve (3)] with temperature T (in K).

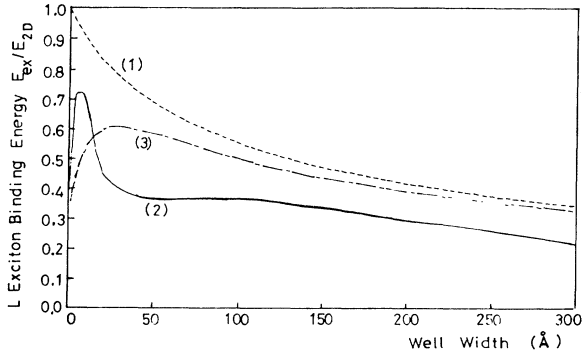

FIG. 6. Light-hole exciton binding energy (in units of 2D exciton binding energy) as a function of well width (in Å). Curve (1) is for the infinite-height barrier well; curve (2) for superlattices; curve (3) for a single well with finite-height barrier.

(L_w), barrier width (L_b), temperature (T), and Al component (x). The transitions Cn-$H(L)n$, $n=1,2,3,4$, are listed in Table II. The results for intersubband transitions $C1$-$C2$ and $C1$-$C3$ are presented in Table III. One can note from Tables II and III that our calculated results agree satisfactorily with the experimental data.[6,9]

Figure 1 shows the variation of the energy spacings between the first conduction subband and the conduction-band edge $\mathcal{E}_{c1}$ with the barrier width L_b. One can see from the figure that $\mathcal{E}_{c1}$ approaches zero as the barrier width L_b goes to zero and approaches a constant as L_b increases beyond a value of 100 Å. The reason is that for $L_b=0$ there is no confinement effect, and when L_b becomes larger, the quantum confinement becomes larger too. When L_b is large enough, the behavior of the superlattice is the same as the single quantum well, and $\mathcal{E}_{c1}$ will be independent of L_b. Figure 2 illustrates the dependence of subband energies $\mathcal{E}_{c1}$, $\mathcal{E}_{h1}$, and $\mathcal{E}_{l1}$ on well width L_w ($\mathcal{E}_{h1}$, $\mathcal{E}_{l1}$ are the energy differences between the valence-band edge and the heavy-, light-hole subbands). In Fig. 2 one can see that $\mathcal{E}_{c1}$, $\mathcal{E}_{h1}$, and $\mathcal{E}_{l1}$ increase as L_w decreases. The results are the same as expected. Figure 3 shows the dependence of $\mathcal{E}_{c1}$, $\mathcal{E}_{h1}$, and $\mathcal{E}_{l1}$ on Al component x. We can find that $\mathcal{E}_{c1}$, $\mathcal{E}_{h1}$, and $\mathcal{E}_{l1}$ increase as the Al component x increases. This is because the Al component x affects the height of the potential barrier and thus affects the quantum-confinement effect. Figure 4 shows the dependence of $\mathcal{E}_{c1}$, $\mathcal{E}_{h1}$, and $\mathcal{E}_{l1}$ on temperature T. One can note that $\mathcal{E}_{c1}$, $\mathcal{E}_{h1}$, and $\mathcal{E}_{l1}$, are almost independent of temperature. This is because the temperature effects the energy gap only.

Figures 5 and 6 present the variation of the exciton binding energies with the well width L_w for heavy and light excitons, respectively. One can see from the figures that both heavy and light excitons exhibit their three-dimensional characters as L_w becomes very large. When L_w decreases, the exciton manifests its two-dimensional character by its large binding energy. For the case of a

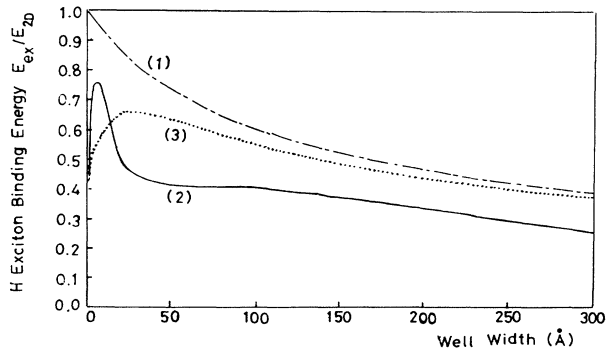

FIG. 5. Heavy-hole exciton binding energy (in units of 2D exciton binding energy) as a function of well width (in Å). Curves (1), (2), and (3) are for infinite-height barrier well, superlattices, and single well with finite-height barriers, respectively.

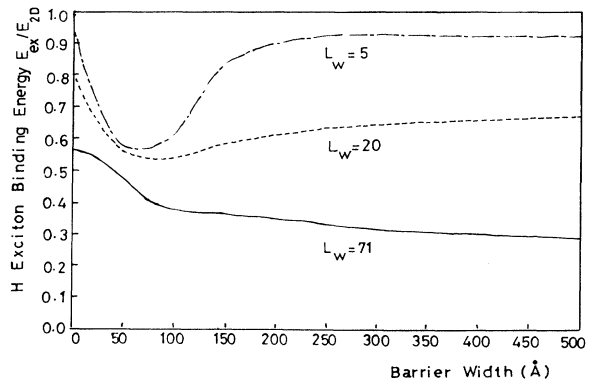

FIG. 7. Heavy-hole exciton binding energy (in units of 2D exciton binding energy) as a function of barrier width (in Å) for three different well widths: $L_w=5$, 20, and 70 Å.

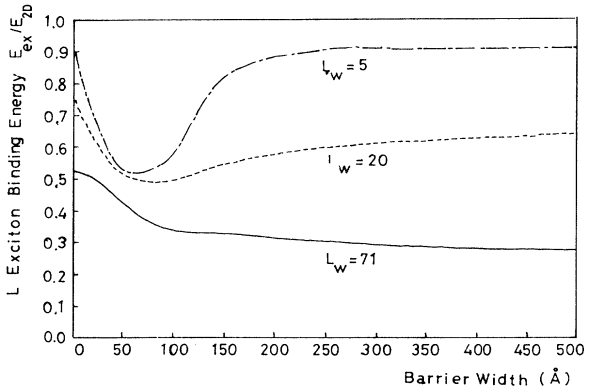

FIG. 8. Light-hole exciton binding energy (in units of 2D exciton binding energy) as a function of barrier width (in Å) for three different well widths: $L_w = 5$, 20, and 70 Å.

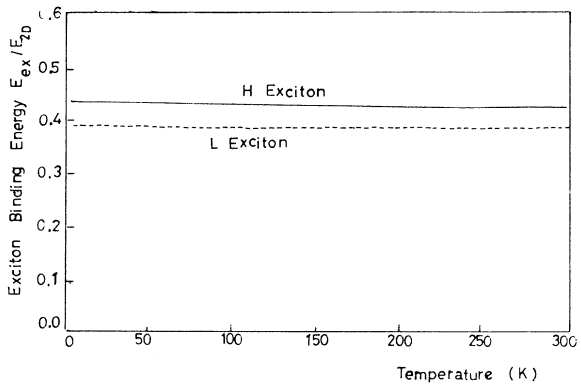

FIG. 10. Variation of the heavy- and light-hole exciton binding energies (in units of 2D exciton binding energy) with temperature T (in K).

finite potential barrier, the behavior of the exciton in a single well or in a superlattice is very different. The binding energy in the latter case has a maximum and decreases rapidly when L_w approaches zero, as can be seen from Figs. 5 and 6. This is because when L_w decreases, the exciton wave function is compressed in the quantum well and thus increases the binding. However, when L_w increases beyond a certain value, the splitting of the wave function in the surrounding $Al_xGa_{1-x}As$ layers becomes important, and this makes the binding energy approach the bulk value of $Al_xGa_{1-x}As$. From Eqs. (6)–(8) we can see that when the well width approaches zero, the probability of finding an exciton in $Al_xGa_{1-x}As$ layers approaches 1. One can note from Figs. 5 and 6 that the exciton binding energy in a superlattice is smaller than that in a single well. This is due to the contribution of coupling of wells in superlattices.

Figures 7 and 8 show the heavy- and light-hole exciton binding energies as a function of barrier width L_b for three different values of well width, namely, $L_w = 5$, 20, and 71 Å. One can note that for small L_w the exciton binding energy $\mathcal{E}_{ex}$ has a minimum when the barrier width is small. A similar result was obtained by Kamizato and Matsuura[3] and Gailbraith and Duggan.[18] For the case of a larger well width, the minimum disappears, and even the barrier width approaches zero. The minimum of the exciton binding energies in the case of smaller L_w is caused from the competition of the following: (i) as the barrier width approaches infinity, the binding energy of the superlattices is equivalent to that of the single quantum well; (ii) as L_b decreases, the exciton binding energy decreases due to the coupling between the neighboring wells. When L_b increases from zero, the electron and hole subband wave functions have dips in the middle of the barrier and thus introduce extra electron-hole separation, which decreases the exciton binding energy. The coupling of wells and extra electron-hole separation produce the opposite effect on exciton binding energy as L_b changes and causes a minimum in the binding-energy curves as shown in Figs. 7 and 8. From Eqs. (6)–(8) one notes that for the smaller well width, tunneling into barrier layers is larger. The coupling of wells is stronger for smaller L_w, and thus can be neglected when L_w is very large. Therefore, the coupling of wells is less important

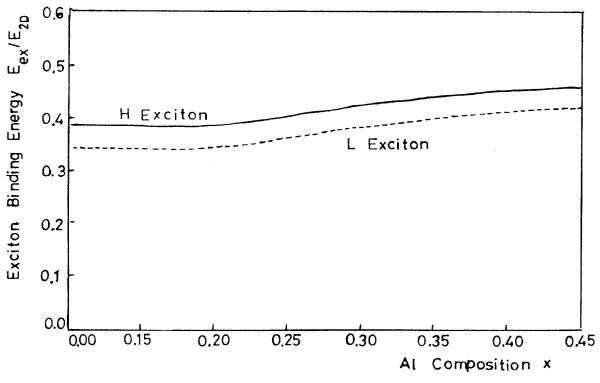

FIG. 9. Variation of the heavy- and light-hole exciton binding energies (in units of 2D exciton binding energy) with Al composition x.

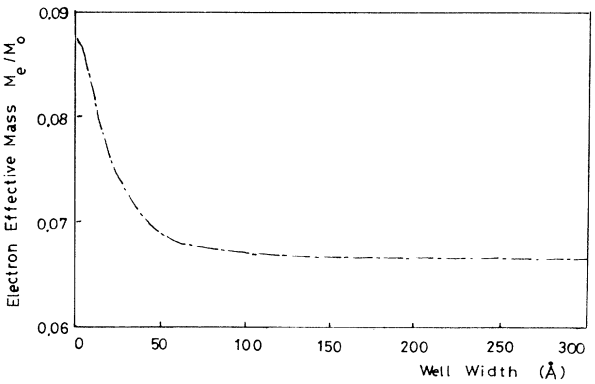

FIG. 11. Variation of the equivalent transverse effective mass m_ρ^* of electrons (in units of the free electron rest mass) with the well width (in Å).

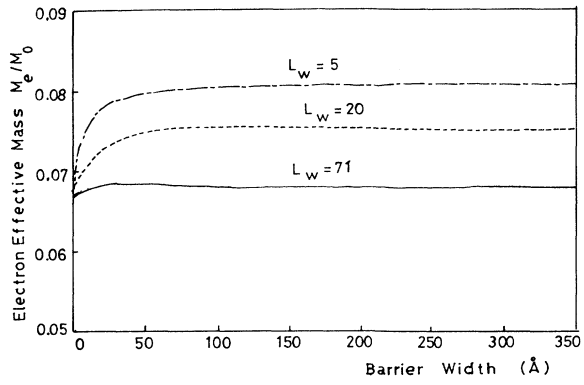

FIG. 12. Variation of equivalent transverse effective mass of electrons (in units of the free electron rest mass) with barrier width (in Å) for three well widths: $L_w = 5$, 20, and 71 Å.

than the extra electron-hole separation for large well width, and the exciton binding energy decreases monotonically as barrier width increases.

If we increase the Al component x, the height of the potential barrier also increases, thus further confining the electron and hole in wells and increasing the exciton binding energy as shown in Fig. 9. Figure 10 shows the dependence of the exciton ground-state binding energy on the temperature. One can see that the effect is very small. This is because the temperature affects the energy gap only, and the energy gap has little effect on the potential barrier. Figures 11 and 12 show the influence of the effective-mass mismatch. The electron equivalent effective mass parallel to the junction $m_{e\rho}^*$ is taken as an example, where $m_{e\rho}^*$ is obtained from Eq. (11). From Fig. 11 one can see that for a larger well width, the equivalent effective mass approaches the value of bulk GaAs, while L_w approaches zero; the equivalent effective mass approaches the value of bulk $Al_xGa_{1-x}As$ as expected. In Fig. 12 we find that for a small well width, the equivalent effective mass increases as the barrier width increases and approaches a constant value when the barrier width is large enough. For the case of a larger well width, the equivalent effective mass is almost independent of barrier width. This is because for the larger well width, the tunneling into barrier layers is smaller. Thus, the equivalent effective mass $m_{e\rho}^*$ approaches the bulk value of $Al_xGa_{1-x}As$ when the barrier width increases. When the well width is large enough, the tunneling effect is very weak and thus the effective mass will become constant.

IV. CONCLUSION

The subband structures and the exciton binding energy of $GaAs/Al_xGa_{1-x}As$ system are studied by the superlattice model and an approximation method, which in some sense combines the spirit of the conventional perturbation method and the variational approach. The exciton binding energy and the energy spacings of the interband and intersubband transitions are calculated within the framework of the effective-mass approximation. Variations of the exciton binding energies with the well width and barrier width for heavy and light excitons are also studied. The effective-mass approximation has been used in this work, and the influence of the effective-mass mismatch is also considered.

The approach used in this work can be applied to study some other systems such as the type-II, modulation-doped, and strained-layer heterostructures. However, it should be mentioned that the merit of our approach relies heavily on a suitable choice of the perturbation term $\mathcal{H}'(\lambda)$ in Eq. (4d). In the case when the electron miniband width is of the same order of magnitude as the exciton binding energy, one has to reorganize the Hamiltonian in such a way that $\mathcal{H}'(\lambda)$ can still be treated as the small perturbation. Otherwise one should include more higher-order correction terms in $\Delta\mathcal{E}_n(\lambda)$ in Eq. (14b) to make the present approach more reliable.

ACKNOWLEDGMENTS

This work was partially supported by the National Science Council of the Republic of China.

[1]R. C. Miller, D. A. Kleinman, and A. C. Gossard, Phys. Rev. B **29**, 7085 (1984).
[2]R. L. Green, K. K. Bajaj, and D. E. Phelps, Phys. Rev. B **29**, 1807 (1984).
[3]T. Kamizato and M. Matsuura, Phys. Rev. B **40**, 8378 (1989).
[4]K. J. Moore, G. Duggan, K. Woodbridge, and C. Roberts, Phys. Rev. B **41**, 1090 (1990); **41**, 1095 (1990).
[5]F. H. Pollak and H. Shen, Superlatt. Microstruct. **6**, 203 (1989).
[6]P. Parayanthal, H. Shen, F. H. Pollak, O. J. Glembocki, B. V. Shanabrook, and W. T. Beard, Appl. Phys. Lett. **48**, 1261 (1986).
[7]R. C. Miller, D. A. Kleinman, O. Munteanu, and W. T. Tsang, Appl. Phys. Lett. **39**, 1 (1981).
[8]W. T. Masselink, P. J. Pearah, J. Klem, C. K. Peng, H. Morkoc, G. D. Sanders, and Y. C. Chang, Phys. Rev. B **32**, 8027 (1985).
[9]Y. C. Chang, J. N. Schulman, G. Bastard, Y. Guldner, and M. Voos, Phys. Rev. B **31**, 2557 (1985).
[10]G. Mo and C. C. Sung, Phys. Rev. B **38**, 1978 (1988).
[11]M. M. Dignam, and J. E. Sipe, Phys. Rev. B **41**, 2865 (1990).
[12]S. Rudiu and T. L. Reinecke, Phys. Rev. B **41**, 3017 (1990).
[13]G. Bastard, E. E. Mendez, L. L. Chang, and L. Esaki, Phys. Rev. B **26**, 1974 (1982).
[14]J. A. Brum and G. Bastard, J. Phys. C **18**, L789 (1985).
[15]N. C. Jarosik, B. D. Mccombe, B. V. Shanabrook, J. Comas, J. Ralston, and G. Wicks, Phys. Rev. Lett. **25**, 1283 (1985).
[16]G. D. Sanders and K. K. Bajaj, Phys. Rev. B **35**, 2308 (1987).
[17]G. Duggan and H. I. Ralph, Phys. Rev. B **35**, 4152 (1987).

[18]I. Galbraith and G. Duggan, Phys. Rev. B **40**, 5515 (1989).
[19]B. R. Salmassi and G. E. W. Bauer, Phys. Rev. B **39**, 1970 (1989).
[20]H. Chu and Y. C. Chang, Phys. Rev. B **39**, 10 861 (1989).
[21]M. Matsuura and Y. Shinozuka, Phys. Rev. B **38**, 9830 (1988).
[22]Y. Shinozuka and M. Martuura, Phys. Rev. B **28**, 4878 (1983); **29**, 3717 (1984).
[23]C. Priester, G. Bastard, G. Allan, and M. Lannoo, Phys. Rev. B **30**, 6029 (1984).
[24]H. Hanken, *Quantum Field Theory of Solids, an Introduction* (North-Holland, Amsterdam, 1976).
[25]Q. G. Zhu and H. Kroemer, Phys. Rev. B **27**, 3519 (1983).
[26]O. Von Roos, Phys. Rev. B **27**, 7547 (1983).
[27]T. Gora and F. Williams, Phys. Rev. **177**, 1179 (1969).
[28]R. A. Morrow and K. R. Brownstein, Phys. Rev. B **30**, 678 (1984).
[29]Y. C. Lee and D. L. Lin, Physica **98A**, 545 (1979).
[30]P. M. Stevenson, Phys. Rev. D **23**, 2916 (1981).
[31]S. Adachi, J. Appl. Phys. **58**, R1 (1985).
[32]D. A. B. Miller, D. S. Chemla, T. C. Damen, A. C. Gassard, W. Wiegman, T. H. Wood, and C. A. Burrus, Phys. Rev. Lett. **53**, 2173 (1984).
[33]R. C. Miller, D. A. Kleinman, W. T. Tsang, and A. C. Gossard, Phys. Rev. B **24**, 1134 (1981).
[34]Y. Fu and K. A. Chao, Phys. Rev. B **40**, 8349 (1989).